

**Determining the potential-dependent identity of methane adsorbates at Pt electrodes using EC-MS**

Journal:	<i>Catalysis Science &amp; Technology</i>
Manuscript ID	CY-ART-08-2023-001172.R1
Article Type:	Paper
Date Submitted by the Author:	30-Sep-2023
Complete List of Authors:	Lucky, Christine; University of Wisconsin-Madison, Chemical and Biological Engineering Fuller, Lee; University of Wisconsin-Madison, Chemistry Schreier, Marcel; University of Wisconsin-Madison, Chemical and Biological Engineering; University of Wisconsin-Madison, Chemistry

## ARTICLE

## Determining the potential-dependent identity of methane adsorbates at Pt electrodes using EC-MS

Received 00th January 20xx,  
Accepted 00th January 20xx

Christine Lucky,<sup>a‡</sup> Lee Fuller<sup>b‡</sup> and Marcel Schreier<sup>a,b\*</sup>

DOI: 10.1039/x0xx00000x

The increased availability of methane resulting from shale gas extraction and renewable feedstocks has made the development of technologies that can utilize this resource in a distributed setting a valuable target. Methane can be leveraged as a resource through its electrochemical partial oxidation to more valuable liquid chemicals, such as methanol, and its total oxidation to generate electricity. Enabling the partial and total oxidation of methane requires an understanding of the surface chemistry of methane under applied potentials. Herein we employ electrochemical mass spectrometry (EC-MS) to investigate the potential-dependent distribution of surface compounds generated from adsorbed methane under ambient conditions. By directly measuring the products of adsorbate oxidation using EC-MS we found that methane adsorption has a strong potential dependence with maximum adsorption at 0.3 V vs RHE, and \*CO is the dominant surface intermediate independent of the potential at which methane is adsorbed. Our findings explain why Pt is a poor catalyst for the electrocatalytic partial oxidation of methane and point the way to better catalysts materials for electrocatalytically valorizing methane in chemical synthesis and electricity generation.

### Introduction

The increased exploitation of shale gas resources and the production of biogas have led to an increased availability of methane. This methane can be used as a fuel, but it can also serve as a cheap and attractive feedstock for chemical synthesis.<sup>1</sup> Methane can be leveraged as a resource through its partial oxidation to more valuable liquid chemicals such as methanol,<sup>2–8</sup> and its total oxidation to generate electricity.<sup>9–11</sup> Yet, methane needs to be converted close to its source since its low volumetric energy density leads to high transportation costs.<sup>12</sup> When transportation is uneconomical, methane is flared on-location, wasting nearly 280 billion cubic feet of methane that could be used for energy generation and chemical production in the United States every year.<sup>13</sup> As a result, there is a need, as well as economic incentive, for technologies that convert methane in a distributed setting.

Oxidizing methane to methanol is attractive because it creates an easily transportable liquid which can be used as either a fuel or a feedstock for further chemical synthesis. However, partial oxidation of methane has proven challenging

since the activation of the first C-H bond requires more energy than the activation of the remaining C-H bonds, resulting in significant overoxidation to CO<sub>2</sub>.<sup>14</sup>

While undesirable in the context of methanol synthesis, the total oxidation of methane can be beneficial when used to produce energy, for example by generating electricity in fuel cells. Solid oxide fuel cells (SOFCs) have been extensively studied for methane oxidation, but their high operating temperature (>700 °C) and infrastructure requirement limit their applicability in the remote and decentralized settings required for natural gas utilization.<sup>11</sup> A promising alternative to SOFCs is the electrochemical oxidation of methane in polymer electrolyte fuel cells (PEFCs), which facilitate conversion at mild temperature and pressure.<sup>9,15,16</sup> The near-ambient operating conditions of electrochemical technologies such as PEFCs open novel avenues of reactivity for methane utilization.

Enabling the partial and total oxidation of methane requires a detailed understanding of the surface chemistry of methane under applied potentials. The electrochemical behaviour of methane has been of interest since the 1960s, when early investigations of hydrocarbon fuel cells were conducted using platinum electrodes.<sup>9,10,17–22</sup> Voltammetric studies found that in acidic electrolyte methane is electrochemically adsorbed at mild potentials as C<sub>1</sub> species, which can be oxidized during an anodic potential sweep.<sup>22–24</sup> Based on similarities to the stripping curves of model compounds, methane was suggested to form a partially oxidized intermediate.<sup>20</sup> Early voltammetric studies refer to this species as “reduced CO<sub>2</sub>” that may<sup>25,26</sup> or may not<sup>22,27</sup>

<sup>a</sup> Department of Chemical and Biological Engineering, University of Wisconsin-Madison, Madison, Wisconsin 53706, United States.

<sup>b</sup> Department of Chemistry, University of Wisconsin-Madison, Madison, Wisconsin 53706, United States.

<sup>‡</sup> These authors contributed equally.

Electronic Supplementary Information (ESI) available: Detailed experiment methods, electrode characterization, and additional results and data. See DOI: 10.1039/x0xx00000x

correspond to  $^*CO$ , with  $^*C-OH$  and  $^*CHO$  proposed as likely alternatives.<sup>22</sup> However, interpretation of voltammetric measurements relies on assumptions about the identity of surface adsorbates. Recent work combining voltammetric measurements with DFT calculations supports the formation of  $^*CO$ .<sup>28,29</sup> Still, voltammetric approaches are insufficient to determine the reaction mechanism or chemical identity of the surface species. Yet, reported measurements using infrared (IR) spectroscopy provide additional ambiguity. While the formation of  $^*CO$  from methane adsorption was observed in several IR spectrometric studies, these works also report signals corresponding to  $^*CHO$ <sup>30,31</sup> and  $^*COOH$ .<sup>31</sup> These findings suggest a more complex adsorbate composition, but the employed measurements are not able to quantify the relative contribution of each intermediate. Additionally, IR studies are limited by selection rules which would prohibit the observation of weaker IR signals related to more reduced  $^*CH_x$  species.<sup>32</sup> To guide the development of methane fuel cells and identify opportunities to promote partial oxidation pathways, reliable insight into the potential-dependent identity of adsorbed methane is needed.

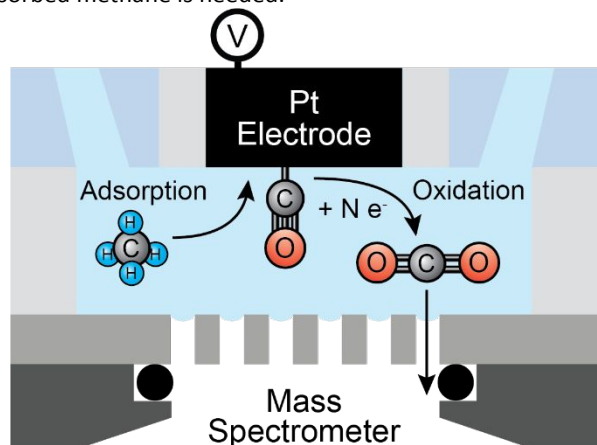


**Figure 1.** Schematic of the EC-MS experiments used to determine the oxidation state of methane adsorbates.

We herein employ electrochemical mass spectrometry (EC-MS) to investigate the potential-dependent distribution of surface compounds generated from adsorbed methane. In EC-MS, an electrochemical interface is brought into close contact with the inlet of a mass spectrometer, allowing for rapid detection of gaseous products.<sup>33,34</sup> We leveraged this capability to investigate the reactivity of methane on a Pt electrode, using EC-MS to track the total oxidation of adsorbed intermediates to CO<sub>2</sub>. By measuring the oxidation products, we determined the quantity of methane adsorbed at different potentials, without relying on assumptions about the identity of adsorbed intermediates. Comparing the amount of CO<sub>2</sub> released upon oxidizing pre-adsorbed methane to the corresponding oxidation charge allowed us to determine the oxidation state of methane-derived surface adsorbates, providing insight into their chemical structure (**Figure 1**). We found that  $^*CO$  is the dominant species across *all adsorption potentials* on Pt, explaining why Pt is a poor catalyst for partial oxidation reactions and providing avenues to the design of

more appropriate catalysts. The insight gained herein will inform future catalyst design to enable decentralized technologies for efficient energy conversion and chemical synthesis from methane and related alkanes.

## Experimental

### Electrode preparation

All experiments were performed using a platinized Pt working electrode prepared using a modified literature method.<sup>35</sup> Briefly, a polished platinum stub was electroplated with nanoporous Pt by contacting the electrode with a solution of 72 mM H<sub>2</sub>PtCl<sub>6</sub> (99.9% trace metals basis, Sigma Aldrich) and 0.13 mM Pb(C<sub>2</sub>H<sub>3</sub>O<sub>2</sub>)<sub>2</sub> (99.999% trace metals basis, Sigma Aldrich) in Milli-Q H<sub>2</sub>O and applying  $-10 \text{ mA cm}^{-2}$  for 10 min using a Pt wire as the counter electrode. After electrodeposition, the Pt stub was gently rinsed in Milli-Q H<sub>2</sub>O before use.

The electrochemical surface area (ECSA) of the electrodeposited Pt stub was calculated using a hydrogen underpotential deposition (H-UPD) method in 1 M HClO<sub>4</sub> (99.999% trace metals basis, Sigma Aldrich). These values were determined by conducting CVs at a scan rate of  $50 \text{ mV s}^{-1}$  and integrating the charge arising from H-UPD using a correlation factor of  $210 \text{ } \mu\text{C cm}^{-2}$  (Figure S1).<sup>28</sup> A Zeiss GeminiSEM 450 using an acceleration voltage of 3.00 kV and an InLens detector was used to image the electrodeposited Pt (**Figure 2a**).

### Methane and carbon monoxide adsorption experiments

Potentiodynamic experiments were carried out under He (Ultra High Purity Grade Helium, Airgas) and using various substrates, including <sup>12</sup>CH<sub>4</sub> (UHP, Airgas), <sup>13</sup>CH<sub>4</sub> (CO-Purified methane, <sup>13</sup>C, 99%, Cambridge Isotope Laboratories), and <sup>12</sup>CO (Research Plus, Airgas). Before carrying out experiments, the electrochemical cell was cleaned in piranha solution (75% H<sub>2</sub>SO<sub>4</sub> and 25% H<sub>2</sub>O<sub>2</sub>) to remove organic impurities, followed by rinsing in Milli-Q water. All experiments were carried out using an EC-MS system from SpectroInlets (Denmark), in a PTFE electrochemical cell placed on top of a semipermeable membrane chip (SpectroInlets, Denmark) that allows for simultaneous supply of substrate gases and diffusion of products into the MS for analysis (Figure S2 & S3). The system was controlled by the proprietary software, Zillien (SpectroInlets, Denmark). 1 M HClO<sub>4</sub> was used as electrolyte, with a Pt wire (99.99%, Kurt J. Lesker Company) counter electrode and Ag/AgCl (3 M KCl, BASi) reference electrode. Potentials were applied using a Biologic SP-200 potentiostat in series with a resistor (100 Ω) to improve signal stability.<sup>36</sup>

Prior to all experiments, the platinized Pt electrode was cleaned by applying a potential of 1.3 V (all potentials reported vs RHE) for 1 min followed by 5 CV cycles between 1.4 and  $-0.05 \text{ V}$  at a scan rate of  $50 \text{ mV s}^{-1}$  in a helium saturated electrolyte. To correct for charge corresponding to the rearrangement of the double layer and any contributions from organic impurities, all experiments consisted of three repetitions of an identical potential program (detailed below). The first two repetitions were performed under helium, while the third was carried out in the presence of substrate methane gas. The second repetition was used for background subtraction. During the experiment, substrate adsorption was carried out for 15 min at the potential of interest before excess

substrate was removed by a helium gas sweep for 15 min at the same potential. Then, the adsorbed species were oxidatively removed as CO<sub>2</sub> using positive-going cyclic voltammetry at a scan rate of 5 mV s<sup>-1</sup>. The vertex potentials were 1.4 V and 0.05 V. A total of 3 CV cycles were performed. For low dose CO experiments, the adsorption potential was held a total of 30 min, but the duration of the substrate exposure was reduced to 1 min. CO stripping was carried out using an identical potential program as used for methane.

We report mass spectrometry signals and voltammetry curves as the difference between experiments in the presence of methane and background values obtained from identical potential-hold experiments conducted only under helium.<sup>28,31</sup> This process is intended to correct for other electrochemical reactions which occur in the potential range of interest, including platinum oxide formation and the oxidation of possible carbon containing contaminants.

#### Calibration of in-situ electrochemical mass spectrometry

MS measurements were calibrated using a two-step procedure consisting of an internal and external calibration. The hydrogen evolution reaction (HER) was used for internal calibration since this reaction can be carried out at 100% Faradaic efficiency on Pt. Because the EC-MS has a collection efficiency of 100% of desorbed products, the measured ionic current can be directly related to the production rate of hydrogen.<sup>34</sup> The internal calibration was performed using a polished Pt stub (99.995%, Pine Instruments) and by applying multiple constant reductive currents until the *m/z* 2 signal stabilized, resulting in an internal hydrogen calibration curve.

Products which cannot be produced with 100% Faradaic efficiency require an external calibration. External calibrations were performed by introducing a known flux of analyte gas into the EC-MS system and measuring the corresponding MS signals. We did this by flowing dilute mixtures of analyte gases in helium into the MS. From the external hydrogen calibration, the resulting H<sub>2</sub> signals were compared to the internal HER calibration to generate H<sub>2</sub> flux vs gas concentration data in the dilute regime. By assuming that the flux of analyte gas is constant to within 0.5 mol% in this regime, calculation of the total flux of gas through the chip capillary is performed using the following equation:

$$\text{He flux into MS} = \frac{(H_2 \text{ signal} - b)/m}{x_{H_2}} \quad (1)$$

Here, *b* is the intercept of the internal HER calibration fit, *m* is its slope, and *x*<sub>H<sub>2</sub></sub> is the mol% of H<sub>2</sub>. The flux of analyte gas through the capillary of the EC-MS chip was determined for other species by assuming constant carrier gas flux. Hydrogen, methane, and <sup>12</sup>CO<sub>2</sub> were calibrated to *m/z* 2, 15, and 44 respectively (Figure S4). For <sup>13</sup>C labelled substrates, *m/z* 45 was used to quantify <sup>13</sup>CO<sub>2</sub>.

## Results and Discussion

### Platinized Pt electrode preparation and characterization

To enable detection of methane oxidation products in EC-MS, we used a high surface area platinized Pt catalyst (Figure 2a). The catalyst was prepared by electrodepositing Pt

from chloroplatinic acid on a polycrystalline Pt disk. We subsequently applied an oxidative potential followed by five CV cycles to clean the electrode prior to experiments. This preparation procedure yielded catalysts with an ECSA of 147 cm<sup>2</sup>, corresponding to a roughness factor of 748 (Table S1). In addition to increasing the surface area available for adsorption, platinization has been suggested to generate a more active catalyst for alkane transformations by lowering the average surface atom coordination number.<sup>28,37</sup>

To determine the activity of the prepared platinized Pt electrodes towards methane oxidation, we first compared the CV traces recorded under both methane and helium (Figure 2b, Figure S5). We did not observe any significant differences between the voltammograms obtained in the presence and absence of methane. These results indicate that although the electrochemical oxidation of methane to CO<sub>2</sub> is thermodynamically favorable at potentials as low as 0.17 V, the process is likely kinetically limited. The voltammogram obtained under methane is consistent with the known CV shape of Pt, indicating that the low amount of generated CO<sub>2</sub> is likely the result of limited adsorption and does not arise from an inert adsorbed layer blocking the surface. H<sub>UPD</sub> and platinum oxide formation remain unaffected, suggesting that these processes are kinetically facile compared to methane activation.

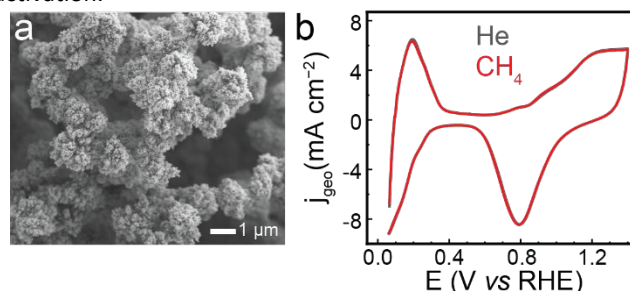
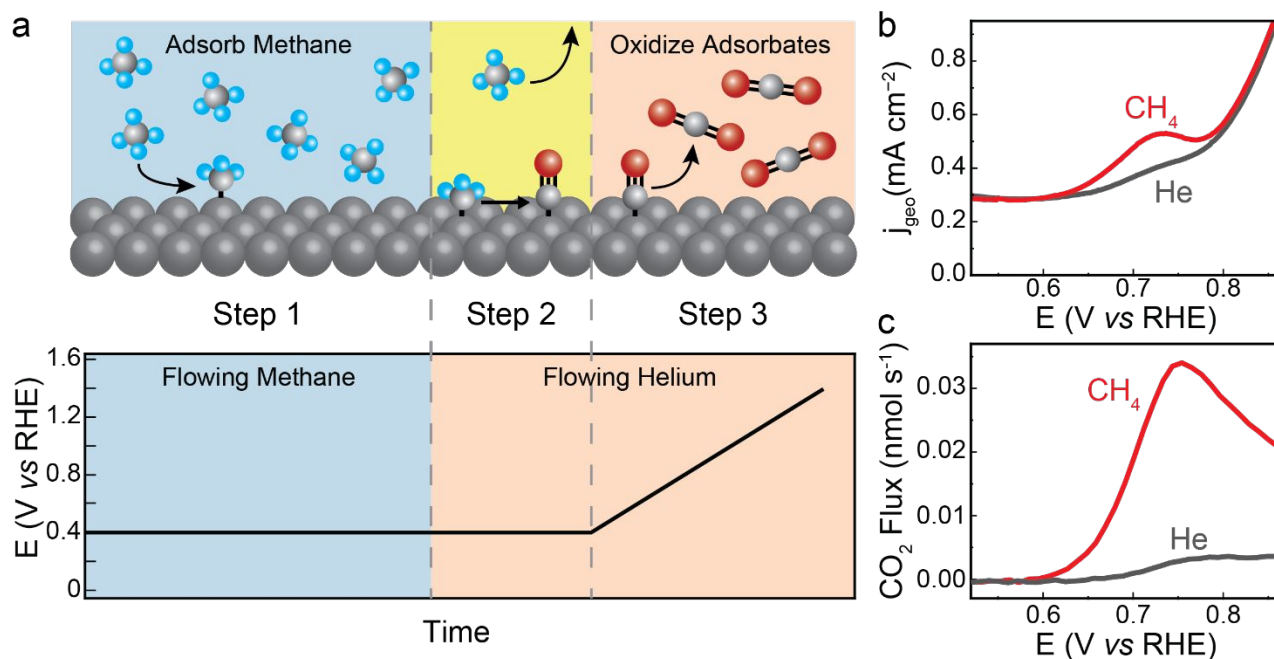


Figure 2. a) SEM image of the high surface area Pt catalyst after electrochemical cleaning. b) Cyclic voltammogram of the as-prepared catalyst in 1 M HClO<sub>4</sub> saturated with helium (gray) and methane (red).

### Electrochemical adsorption and oxidation of methane

To generate insight into the identity of methane adsorbates, we first required sufficient surface coverage to perform characterization experiments. We therefore adsorbed CH<sub>4</sub> prior to oxidative stripping. In our experiments, we adsorbed methane at different potentials for 15 minutes. We then removed the remaining substrate with a helium sweep to ensure that we only examined the transformation of surface bound species (Figure 3). We then applied an anodic potential sweep at 5 mV s<sup>-1</sup> to initiate the total oxidation of any adsorbed species, while simultaneously monitoring the generated CO<sub>2</sub>. Combining the CO<sub>2</sub> measurements with the charge passed during oxidation allowed us to elucidate the identity of adsorbed intermediates as described below.



**Figure 3.** a) Overview of the experimental procedure where methane is first adsorbed for 15 min before being removed from solution and the resulting adsorbates are oxidized to CO<sub>2</sub> in a potential sweep. b) Cyclic voltammetry showing the oxidation peak after adsorbing methane (red) compared to a control performed under helium (gray). c) The CO<sub>2</sub> produced during oxidative stripping after the adsorption of methane (red) and an identical experiment under helium (gray). Full potential range shown in Figure S6.

The CV sweep following adsorption at 0.3 V shows that methane derived adsorbates give rise to a single oxidation feature with a peak at 0.73 V (Figure 3b). This is consistent with previous voltammetric studies of methane oxidation.<sup>10,28,29,31</sup> The oxidation feature in the current is accompanied by a single peak of generated CO<sub>2</sub> at the same potential (Figure 3c and Figure S6), indicating that the passed charge is associated with a total oxidation process. The second CV cycle did not include any methane oxidation features demonstrating that all of the adsorbed methane was removed during oxidation (Figure S7). Our method therefore provides direct and accurate quantification of the amount of adsorbed methane.

#### Potential dependence of methane adsorption

To characterize the effect of potential on methane adsorption, we quantified the CO<sub>2</sub> produced during oxidative stripping following methane adsorption at a series of applied voltages. The CO<sub>2</sub> produced after adsorbing methane for 15 min at potentials ranging from 0.25 to 0.5 V are shown in Figure 4. Our results indicate that methane adsorption reaches a maximum at 0.3 V, in agreement with previous studies of short chain alkane adsorption in acidic electrolytes.<sup>36,38,39</sup> While the maximum adsorption potential is within the range reported for methane activation under varying operating conditions (0.26 – 0.3 V),<sup>10,22,40</sup> it is slightly lower than the maximum of 0.4 V reported by Boyd et. al. for a similar system where adsorption was quantified via the charge required to oxidize all adsorbates.<sup>28</sup> At more oxidative and reductive potentials methane adsorption decreases steeply, with no

quantifiable adsorption at potentials of 0.2 and 0.6 V after 15 min (Figure S8).

The potential dependence of methane adsorption can be explained by a combination of the thermodynamics of the electrochemical interface and surface coverage effects. The thermodynamics of adsorption at electrified interfaces are described by the Gibbs adsorption isotherm, which stipulates that the interfacial concentration of neutral species, such as methane, is maximized when the interfacial drop in the electrostatic potential is at a minimum.<sup>41</sup> These conditions occur at the potential of zero charge (PZC), which is reported

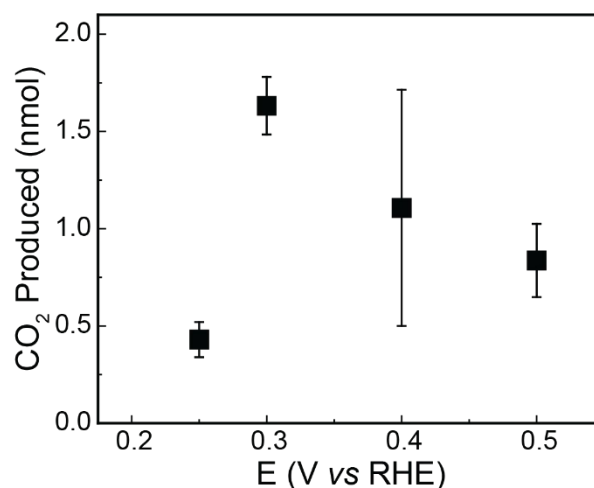


**Figure 4.** The amount CO<sub>2</sub> produced upon oxidizing the methane adsorbed in 15 min at different potentials using a 1 M HClO<sub>4</sub> electrolyte. All points are the average of at least three trials with error bars representing one standard deviation. Representative oxidative stripping traces at each potential are shown in Figure S9 and values of all individual trials shown in Figure S10.

to be near 0.3 V in HClO<sub>4</sub> and coincides with our observed maximum in adsorption.<sup>42</sup> Furthermore, at 0.3 V a greater proportion of surface sites are free of competing adsorbates than at more reductive or oxidative potentials where surface hydrogen or hydroxide/oxygen species begin to compete with available active sites.<sup>28</sup>

#### Adsorbate oxidation state as a function of electrode potential

To determine whether the applied potential controls the chemical identity of the adsorbed methane, we measured the oxidation state of the surface species resulting from adsorption at each adsorption potential. This was made possible by calculating the number of electrons needed to produce one molecule of CO<sub>2</sub> through the total oxidation of surface adsorbates (Equation 2).<sup>43–45</sup> This value, which we term *N*, is calculated as follows:

$$N = \frac{n_{e^-}}{n_{CO_2}} \quad (2)$$

Here,  $n_{e^-}$  is the number of electrons transferred during the oxidative peak and  $n_{CO_2}$  is the number of CO<sub>2</sub> molecules generated as a result. Unlike spectroscopic methods used in previous studies, calculation of the oxidation state is agnostic to IR selection rules and active sites and thus allows us to interrogate the possible presence of \*CH<sub>x</sub> species on the surface, which would result in a higher *N* than oxygenated adsorbates. **Figure 5** shows the *N* values corresponding to a series of possible intermediates formed from the adsorption of CH<sub>4</sub> to a Pt surface. The *N* values are diagnostic for an intermediate and thus allow us to suggest the structure of adsorbed methane.

We validated this method by oxidizing a monolayer of CO adsorbed at 0.3 V. This resulted in an experimental *N* value of 2.08 ± 0.06, which agrees with the expected value of 2 shown in **Figure 5** (Table S2).

Measuring the oxidation state of adsorbed methane suggested that \*CO is the dominant intermediate formed at all potentials between 0.25 and 0.5 V. As shown in **Figure 6**, the adsorbates resulting from methane activation had an *N* value of 2.4–2.7. We did not observe any significant variation of the oxidation state with adsorption potential, suggesting that while methane adsorption is a potential dependent process its subsequent reaction on the surface is not. While the measured

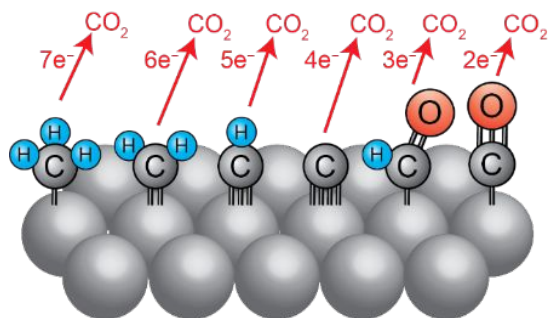


**Figure 5.** Possible methane-derived surface species and their corresponding *N* values.

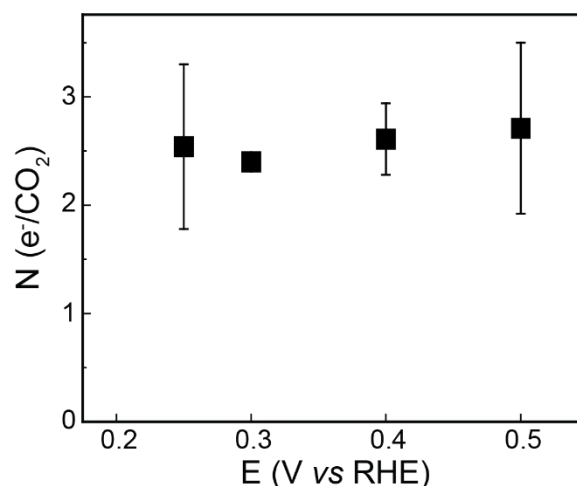


**Figure 6.** The *N* value for <sup>12</sup>CH<sub>4</sub>-derived surface species following a 15 min adsorption at various potentials. All points are the average of at least three trials with error bars representing one standard deviation. Individual trials shown in Figure S10.

oxidation state deviates from that measured of a \*CO monolayer, a value below 3 necessitates the presence of \*CO on the surface. While adsorbed formate also has an *N* of 2, it has been shown to undergo dehydration to form \*CO in the potential range of interest and is not expected to be present in significant amounts (Figure S12).<sup>29,46–49</sup> The experimental *N* value represents the average oxidation state of all adsorbed carbon. Thus, it is possible that a small population of more reduced species remains present at the surface. This would agree with prior voltametric studies which suggest greater than 2 electrons per covered site are needed for total oxidation.<sup>22</sup>

To evaluate the proportion of adsorbate which can be attributed to \*CO at the maximum adsorption potential of 0.3 V, we determined what linear combination of \*CO and other possible species gives rise to our observed *N* value. For example, multiple reports suggested that methane could form \*CHO, which would have an *N* of 3.<sup>30,31</sup> If we assume that \*CO and \*CHO are the only species present at 0.3 V, we obtain a lower bound on the fraction of adsorbed methane, which indicates that at least 60% of adsorbates are \*CO (calculation details in Supporting Information). Conversely, to find the upper bound on the fraction of \*CO, we assume that the remaining species are at the most reduced state previously reported. Studies indicated that \*CH<sub>2</sub>, which has an *N* value of 6, might remain stable on Pt(110) surfaces under mildly oxidative potentials.<sup>29</sup> Considering the adsorbate as a combination of only \*CO and \*CH<sub>2</sub> we obtain an upper bound of 90% \*CO.

The increase in *N* for methane derived adsorbates compared to CO may also be correlated with the surface coverage. We note that the \*CO monolayer experiments used to qualify the *N* method had approximately 100 times the coverage of the methane oxidation experiments. Accounting for the presence of organic impurities by subtracting the CO<sub>2</sub> produced in the preceding control from that produced after methane adsorption is likely to underestimate  $n_{CO_2}$  and

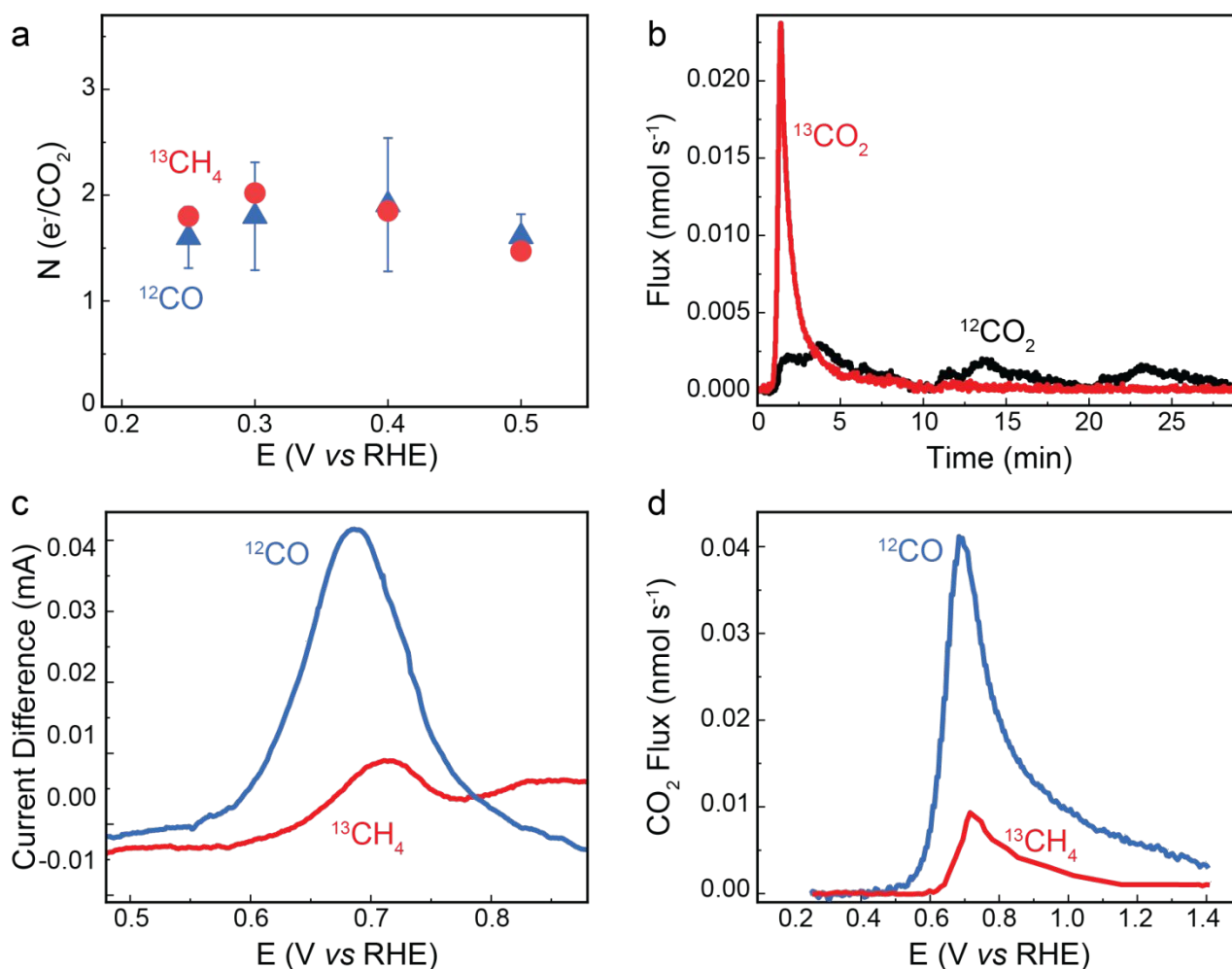


**Figure 7.** a) Comparison of the  $N$  values of  $^{13}\text{CH}_4$ -derived surface species (red) and  $^{12}\text{CO}$ -derived surface species at low coverage (blue). The  $\text{CO}$  measurements show the average of at least 3 trials with error bars representing one standard deviation. b) The flux of  $^{13}\text{CO}_2$  and  $^{12}\text{CO}_2$  during the three CV cycles following  $^{13}\text{CH}_4$  adsorption showing the relative contribution of methane derived species and organic impurities. c) The current difference and d)  $\text{CO}_2$  produced during the oxidative stripping of  $^{13}\text{CH}_4$  (red) and  $^{12}\text{CO}$  (blue) derived surface species. Representative traces at each potential shown in Figure S11.

consequently increase the  $N$  value. This impact would be more prominent at low coverages.

To verify that our data is not convoluted by putative organic impurities in the electrolyte solution, we repeated our experiments with  $^{13}\text{CH}_4$  as substrate. Using  $^{13}\text{C}$ -labeled methane allowed us to avoid background subtraction by excluding the impact of organic impurities, which give rise to  $^{12}\text{CO}_2$  during repeated CV cycles following adsorption and can convolute measurements (Figure 7b). The  $^{13}\text{CH}_4$  experiments resulted in  $N$  values close to 2, supporting formation of  $^*\text{CO}$  at all adsorption potentials. To exclude that our measurements are convoluted by coverage effects, which are known to shift the peak position of  $\text{CO}$  oxidation, we compared our data to oxidation experiments carried out with a  $\text{CO}$  coverage comparable to the one estimated from  $\text{CH}_4$  adsorption.<sup>50–53</sup> These experiments showed strong agreement between the oxidation state of methane derived adsorbates and  $^*\text{CO}$  (Figure 7a). Furthermore, the onset potential of oxidation and  $\text{CO}_2$  generation from adsorbed methane and adsorbed  $\text{CO}$  coincide (Figure 7c & d). Overall, the minimal variation in  $N$

value with potential suggests that  $^*\text{CO}$  is the dominant intermediate formed from methane even at potentials as low as 0.25 V. While this oxygenation occurs at potentials where  $^*\text{OH}$  is thought to be absent from the surface,<sup>54</sup> previous reports also suggest the formation of oxygenates at similarly reductive potentials.<sup>10,16,22–24,28,30,31,55,56</sup> We attribute the formation of  $^*\text{CO}$  at these driving forces to the strength of the Pt-CO bond. This observation is supported by previous DFT calculations, which showed that  $^*\text{CO}$  is the most stable intermediate in the total methane oxidation pathway for applied potentials between 0.17 and 0.6 V.<sup>28</sup> We hypothesized that formation of strongly bound  $\text{CO}$  provides the driving force to facilitate the rapid dehydrogenation and oxygenation of methane. While this behavior makes Pt a favorable oxidation catalyst, it hinders the development of partial oxidation pathways where the formation of  $^*\text{CO}$  is unfavorable. Our finding that  $^*\text{CO}$  is the dominant methane-derived surface species at all measurable potentials is consistent with results obtained through voltammetric and spectroscopic methods.<sup>28,29,31</sup> These observations suggest a potential-

independent methane oxidation mechanism and indicate that other catalyst materials should be considered when pursuing partial oxidation routes.

These findings provide guidance for the development of methane oxidation catalysts. The facile formation of \*CO on Pt surfaces, even at low driving forces suggests that the onset potential of methane oxidation is determined by the oxidation of \*CO. Studies of CO oxidation have found that alloying Pt with oxophilic metals, such as Sn, can lower the oxidation onset potential by up to 400 mV.<sup>57–60</sup> We suggest that similar approaches could be used to lower the overpotential losses in methane fuel cells. Conversely, the production of partially oxidized products is inhibited by \*CO formation, which cannot be hydrogenated on Pt. Materials which bind \*CO more weakly while still facilitating methane activation would be attractive candidates for partial oxidation catalysts. While most transition metals do not achieve these criteria,<sup>28</sup> a combination of materials engineering and the development of alternative reaction schemes may facilitate pathways for electrocatalytic methane partial oxidation.

## Conclusions

Understanding the surface species formed during the electrocatalytic oxidation of methane on Pt is vital for accessing and developing new pathways to utilize this valuable carbon resource. Here, we employed EC-MS to probe the oxidation state of methane-derived intermediates through simultaneous quantification of the oxidizing charge and resulting CO<sub>2</sub>. Using this approach, we found that adsorption is maximized at 0.3 V with \*CO being the dominant surface species across all tested adsorption potentials from 0.25 to 0.5 V. We attribute this behaviour to the strong binding of \*CO on Pt, which creates a strong driving force for rapid dehydrogenation and oxygenation of adsorbed methane. Our results explain why Pt is a poor catalyst for the partial oxidation of CH<sub>4</sub> and they provide avenues for designing more efficient CH<sub>4</sub> fuel cell catalysts.

## Author Contributions

‡ These authors contributed equally.

## Conflicts of interest

There are no conflicts to declare.

## Acknowledgements

We acknowledge a Seed Grant through the Wisconsin Materials Research Science and Engineering Center (DMR-1720415). The authors acknowledge support by the Arnold and Mabel Beckman Foundation through a Beckman Young Investigator Award and by the ACS Petroleum Research Fund. We also acknowledge use of facilities and instrumentation at the UW-Madison Wisconsin Centers for Nanoscale Technology

partially supported by the NSF through the University of Wisconsin Materials Research Science and Engineering Center (DMR-1720415). This material is based upon work supported by the National Science Foundation Graduate Research Fellowship Program under Grant No. DGE- 2137424. Any opinions, findings, and conclusions or recommendations expressed in this material are those of the authors and do not necessarily reflect the views of the National Science Foundation. Support was also provided by the Graduate School and the Office of the Vice Chancellor for Research and Graduate Education at the University of Wisconsin-Madison with funding from the Wisconsin Alumni Research Foundation. The authors also acknowledge support from the University of Wisconsin-Madison and the Wisconsin Alumni Research Foundation.

## References

- 1 E. McFarland, *Science*, 2012, **338**, 341–342.
- 2 T. J. Omasta, W. A. Rigdon, C. A. Lewis, R. J. Stanis, R. Liu, C. Q. Fan and W. E. Mustain, *ECS Trans.*, 2015, **66**, 129–136.
- 3 A. A. Latimer, A. Kakekhani, A. R. Kulkarni and J. K. Nørskov, *ACS Catal.*, 2018, **8**, 6894–6907.
- 4 S. Grundner, M. A. C. Markovits, G. Li, M. Tromp, E. A. Pidko, E. J. M. Hensen, A. Jentys, M. Sanchez-Sanchez and J. A. Lercher, *Nat. Comm.*, 2015, **6**, 1–9.
- 5 J. S. Woertink, P. J. Smeets, M. H. Groothaert, M. A. Vance, B. F. Sels, R. A. Schoonheydt and E. I. Solomon, *PNAS USA*, 2009, **106**, 18908–18913.
- 6 M. H. Groothaert, P. J. Smeets, B. F. Sels, P. A. Jacobs and R. A. Schoonheydt, *J. Am. Chem. Soc.*, 2005, **127**, 1394–1395.
- 7 K. Narsimhan, K. Iyoki, K. Dinh and Y. Román-Leshkov, *ACS Cent. Sci.*, 2016, **2**, 424–429.
- 8 R. A. Periana, D. J. Taube, S. Gamble, H. Taube, T. Satoh and H. Fujii, *Science*, 1998, **280**, 560–564.
- 9 M. L. Perry and T. F. Fuller, *J. Electrochem. Soc.*, 2002, **149**, S59.
- 10 L. W. Niedrach, *J. Electrochem. Soc.*, 1966, **113**, 645–650.
- 11 M. Stoukides, *J. Appl. Electrochem.*, 1995, **25**, 899–912.
- 12 G. Molnar and G. Molnar, *The Palgrave Handbook of International Energy Economics*, 2022, 23–57.
- 13 Natural Gas Vented and Flared, [https://www.eia.gov/dnav/ng/ng\\_prod\\_sum\\_a\\_EPGO\\_VGV\\_mm\\_cf\\_a.htm](https://www.eia.gov/dnav/ng/ng_prod_sum_a_EPGO_VGV_mm_cf_a.htm), (accessed 31 July 2023).
- 14 J. A. Labinger, *J. Mol. Catal. A*, 2004, **220**, 27–35.
- 15 P. Jacquinet, B. Müller, B. Wehrli and P. C. Hauser, *Anal. Chim. Acta*, 2001, **432**, 1–10.
- 16 L. W. Niedrach, *J. Electrochem. Soc.*, 1966, **113**, 645.
- 17 L. W. Niedrach, *J. Electrochem. Soc.*, 1964, **111**, 1309–1317.
- 18 L. W. Niedrach and M. Tochner, *J. Electrochem. Soc.*, 1967, **114**, 233.
- 19 W. T. Grubb and L. W. Niedrach, *J. Electrochem. Soc.*, 1963, **110**, 1086.
- 20 L. W. Niedrach, S. Gilman and I. Weinstock, *J. Electrochem. Soc.*, 1965, **112**, 1161–1166.
- 21 S. B. Brummer, in *Fuel Cell Systems - II*, ed. R. F. Gould, American Chemical Society, Washington DC, 1969, pp. 223–230.
- 22 A. H. Taylor and S. B. Brummer, *J. Phys. Chem.*, 2002, **73**, 2397–2403.
- 23 A. H. Taylor and S. B. Brummer, *J. Phys. Chem.*, 1968, **72**, 2856–2862.
- 24 A. Y. Tsivadze, O. E. Aksyutin and A. G. Ishkov, *J. Electrochem. Soc.*, 1966, **113**, 645.
- 25 M. W. Breiter, *Electrochim. Acta*, 1967, **12**, 1213–1218.

- 26 T. Biegler, *J. Phys. Chem.*, 1968, **72**, 1571–1577.
- 27 S. B. Brummer and K. Cahill, *Discuss Faraday Soc.*, 1968, **45**, 67–78.
- 28 M. J. Boyd, A. A. Latimer, C. F. Dickens, A. C. Nielander, C. Hahn, J. K. Nørskov, D. C. Higgins and T. F. Jaramillo, *ACS Catal.*, 2019, **9**, 7578–7587.
- 29 H. Bin Ma, T. Sheng, W. S. Yu, J. Y. Ye, L. Y. Wan, N. Tian, S. G. Sun and Z. Y. Zhou, *ACS Catal.*, 2019, **9**, 10159–10165.
- 30 F. Hahn and C. A. Melendres, *Electrochim. Acta*, 2001, **46**, 3525–3534.
- 31 S. M. Gurses and C. X. Kronawitter, *J. Phys. Chem. C*, 2021, **125**, 2944–2955.
- 32 D. W. Flaherty, D. D. Hibbitts, E. I. Gürbüz and E. Iglesia, *J. Catal.*, 2014, **311**, 350–356.
- 33 H. Baltruschat, *J. Am. Soc. Mass Spectrom.*, 2004, **15**, 1693–1706.
- 34 D. B. Trimarco, S. B. Scott, A. H. Thilsted, J. Y. Pan, T. Pedersen, O. Hansen, I. Chorkendorff and P. C. K. Vesborg, *Electrochim. Acta*, 2018, **268**, 520–530.
- 35 A. M. Feltham and M. Spiro, *Chem. Rev.*, 1971, **71**, 177–193.
- 36 H. B. Bakshi, C. Lucky, H. S. Chen and M. Schreier, *J. Am. Chem. Soc.*, 2023, **145**, 13742–13749.
- 37 T. Jiang, D. J. Mowbray, S. Dobrin, H. Falsig, B. Hvolbæk, T. Bligaard and J. K. Nørskov, *J. Phys. Chem. C*, 2009, **113**, 10548–10553.
- 38 S. Gilman, *Trans. Faraday Soc.*, 1965, **61**, 2546–2560.
- 39 J. A. Shropshire and H. H. Horowitz, *J. Electrochem. Soc.*, 1966, **113**, 490–495.
- 40 M. G. Sustersic, R. Córdova, W. E. Triaca and A. J. Arvia, *J. Electrochem. Soc.*, 1980, **127**, 1242–1248.
- 41 B. J. Piersma, in *Electrosorption*, ed. E. Gileadi, Plenum Press, New York, NY, 1967, pp. 19–49.
- 42 K. Ojha, N. Arulmozhi, D. Aranzales and M. T. M. Koper, *Angew. Chem. Int. Ed. Engl.*, 2020, **59**, 711.
- 43 J. F. E. Gootzen, A. H. Wonders, W. Visscher and J. A. R. Van Veen, *Langmuir*, 1997, **13**, 1659–1667.
- 44 S. Bruckenstein and J. Comeau, *Faraday Discuss. Chem. Soc.*, 1973, **91**, 285–292.
- 45 W. T. Grubb and M. E. Lazarus, *J. Electrochem. Soc.*, 1967, **114**, 360–361.
- 46 E. Herrero and J. M. Feliu, *Curr. Opin. Electrochem.*, 2018, **9**, 145–150.
- 47 W. Gao, J. A. Keith, J. Anton and T. Jacob, *J. Am. Chem. Soc.*, 2010, **132**, 18377–18385.
- 48 G. Samjeské, A. Miki, S. Ye and M. Osawa, *J. Phys. Chem. B*, 2006, **110**, 16559–16566.
- 49 Y. X. Chen, A. Miki, S. Ye, H. Sakai and M. Osawa, *J. Am. Chem. Soc.*, 2003, **125**, 3680–3681.
- 50 A. López-Cudero, A. Cuesta and C. Gutiérrez, *J. Electroanal. Chem.*, 2005, **579**, 1–12.
- 51 E. Grantscharova-Anderson and A. B. Anderson, *Electrochim. Acta*, 1999, **44**, 4543–4550.
- 52 T. Sato, K. Kunitatsu, H. Uchida and M. Watanabe, *Electrochim. Acta*, 2007, **53**, 1265–1278.
- 53 M. J. S. Farias, W. Cheuquepán, A. A. Tanaka and J. M. Feliu, *ACS Catal.*, 2020, **10**, 543–555.
- 54 J. Clavilier, R. Albalat, R. Gomez, J. M. Orts, J. M. Feliu and A. Aldaz, *J. Electroanal. Chem.*, 1992, **330**, 489–497.
- 55 S. B. Brummer and M. J. Turner, *J. Phys. Chem.*, 1967, **71**, 3902–3906.
- 56 H. Ma, P. Hao, J.-Y. Ye, Z.-Y. Zhou and S.-G. Sun, *Journal of Electroanalytical Chemistry*, 2021, **896**, 115252.
- 57 S. Stevanović, D. Tripković, V. Tripković, D. Minić, A. Gavrilović, A. Tripković and V. M. Jovanović, *J. Phys. Chem. C*, 2014, **118**, 278–289.
- 58 M. Chen, Y. Han, T. W. Goh, R. Sun, R. V. Maligal-Ganesh, Y. Pei, C. K. Tsung, J. W. Evans and W. Huang, *Nanoscale*, 2019, **11**, 5336–5345.
- 59 H. Huang, O. F. Blackman, V. Celorrio and A. E. Russell, *Electrochim. Acta*, 2021, **390**, 138811.
- 60 W. D. Michalak, J. M. Krier, S. Alayoglu, J. Y. Shin, K. An, K. Komvopoulos, Z. Liu and G. A. Somorjai, *J. Catal.*, 2014, **312**, 17–25.